The coupling effect of air-bridges on broadband spiral inductors in SiC-based MMIC technology*

Jia-Xin Zheng(郑佳欣)[1], Xiao-Hua Ma(马晓华)[1,†], Yang Lu(卢阳)[2], Bo-Chao Zhao(赵博超)[2], Heng-Shuang Zhang(张恒爽)[2], Meng Zhang(张濛)[1], Li-Xiang Chen(陈丽香)[1], Qing Zhu(朱青)[1], and Yue Hao(郝跃)[2]

[1] *School of Advanced Material and Nanotechnology, Xidian University, Xi'an* 710071, *China*
[2] *School of Microelectronics, Xidian University, Xi'an* 710071, *China*

(Received 20 March 2017; revised manuscript received 3 May 2017; published online 10 July 2017)

The coupling effect of air-bridges on broadband spiral inductors in SiC-based MMIC technology has been investigated deeply. The fabricated 1-nH spiral inductor on SiC substrate demonstrates a self-resonant frequency of 51.6 GHz, with a peak *Q*-fact of 12.14 at 22.1 GHz. From the *S*-parameters measurements, the exponential decay phenomenon is observed for *L*, *Q*-factor, and SRF with the air-bridge height decreasing, and an analytic expression is concluded to exactly fit the measured data which can be used to predict the performance of the spiral inductor. All the coefficients in the formula have specific meaning. By means of establishing the lumped model, the parasitic coupling capacitance of the air-bridge has been extracted and presents the exponential decay with the air-bridge heights decreasing which indicates that this capacitor is directly related to the coupling effect of the air-bridge. Through the electromagnetic field distribution simulation, the details of the electric field around the air-bridge have been presented which demonstrate the formation and the variation principles of the coupling effect.

Keywords: coupling effect, air-bridge, broadband spiral inductor, exponential decay, SiC, MMIC

PACS: 84.32.–y, 84.32.Hh, 84.40.Dc, 85.30.De **DOI:** 10.1088/1674-1056/26/8/088401

1. Introduction

Microstrip spiral inductors are important passive components for radio frequency (RF) chocking, tuning, matching and filtering and are extensively used in monolithic microwave integrated circuits (MMIC) design. Large amounts of experimental and theoretical work have been done to investigate the characteristics of microwave spiral inductors on different substrate. In Ref. [1], an air-bridge based on-chip suspended inductor on sapphire has been proposed. With lower parasitic capacitance and smaller substrate loss, the *Q*-factor has been improved to 10.6, with a self-resonant frequency of 10 GHz. In Ref. [2], spiral inductors have been fabricated by using copper-damascene interconnects on high-resistivity silicon (HRS) and sapphire substrates. The 1.4-nH inductors have *Q*-factors of 30 at 5.2 GHz and 40 at 5.8 GHz for the HRS and the sapphire substrates, respectively. Abundant spiral inductors based on GaAs[3,4] and low-resistivity silicon[5–7] substrates with different structures have been investigated intensively and outstanding performances have been reported. With smaller relative dielectric constant and higher thermal conductivity, the parasitic capacitance of the SiC-based devices and circuits is smaller and the thermal reliability of them is improved. With these advantages, SiC can be a splendid candidate for high frequency and high power applications. It is an ideal substrate for AlGaN/GaN heterojunction epitaxy,[8,9] because SiC has excellent thermal conductivity and superior lattice matching with GaN material. So SiC-based GaN MMIC has a good prospect in power and microwave applications. But the spiral inductors based on SiC substrate have never been individually reported before.

The goals of inductor design for MMIC applications are large inductance with small size, high *Q*-factor and high self-resonant frequency (SRF). The performances of the spiral inductors are limited by the conductor losses,[10] the substrate losses,[11] and the coupling effect between the microstrip lines.[12] Moreover, the coupling effect of the air-bridge also has a significant effect on the inductor performance, because the air-bridge, the underpass line and the dielectric between them can effectively form parallel-plate capacitors and these shunt capacitors will deteriorate the inductance, the resonant frequency, and the *Q*-factor in a certain way. But as far as the authors know, the mechanism of the air-bridge coupling effect has not attracted enough attention and seldom been investigated before.

In this paper, planar spiral inductors with air-bridges have been fabricated on 4H–SiC substrate and the coupling effect of air-bridges has been explored in detail. The fabricated spiral inductor on SiC substrate demonstrates a self-resonant

*Project supported by the National Natural Science Foundation of China (Grant Nos. 61334002 and 61474091) and the National High Technology Research and Development Program of China (Grant No. 2015AA016801).

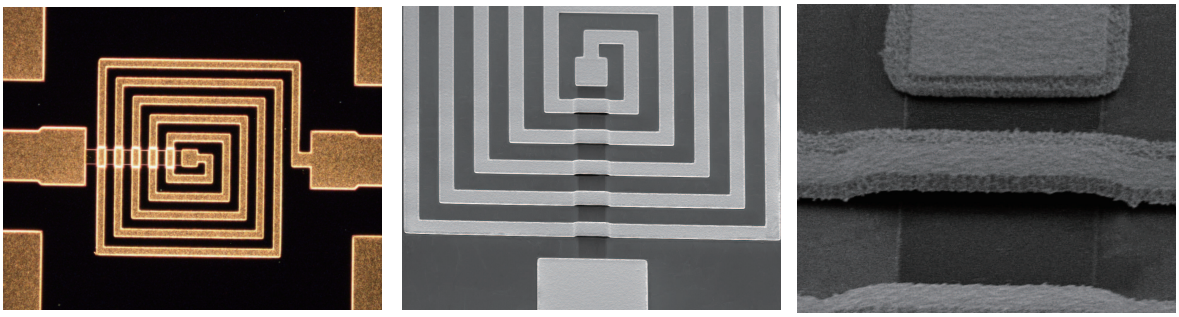
†Corresponding author. E-mail: xhma@xidian.edu.cn

© 2017 Chinese Physical Society and IOP Publishing Ltd

frequency of 51.6 GHz, with a peak Q-factor of 12.14 at 22.1 GHz. From the S-parameters measurements, the exponential decay phenomenon is observed for L, Q, and SRF with the air-bridge height decreasing, and an analytic expression is concluded to fit the measured data exactly which can be used to predict the performance of the spiral inductor. All the coefficients in the formula have specific meaning. The parasitic capacitor for the coupling effect of the air-bridge has been extracted based on the lumped model and the field distribution in the air-bridge area has been calculated by electromagnetic (EM) simulation. The Q-factor, inductance, and self-resonant frequency dependence of the air-bridge height has been discussed.

2. The fabrication of the on-chip spiral inductor and the measurement results

Figure 1(a) shows the microphotograph of the fabricated on-chip spiral inductor on 100-μm-thick 4H–SiC substrate. The underpass line metal Ti/Au with a thickness of 20 nm/400 nm was evaporated and then the 200-nm-thick SiN dielectric layer was deposited by plasma enhanced chemical vapor deposition (PECVD). Then the via-hole for the interconnection between the underpass line and the top spiral metal was etched by inductively coupled plasma (ICP). The 3-μm-thick Au of the top metal was electroplated and the substrate was thinned to 100 μm and electroplated again from the backside. Figures 1(b) and 1(c) show the SEM images of the air-bridges and the single air-bridge structure.



(a) (b) (c)

Fig. 1. (color online) (a) The microphotograph of the fabricated on-chip spiral inductors on SiC substrate, (b) the scanning electron microscopy (SEM) image of the air-bridges, and (c) the SEM image of a single air-bridge.

To investigate the coupling effect of the air-bridge, spiral inductors with different air-bridge heights are fabricated with coplanar waveguide to microstrip transitions and measured by the vector network analyzer. Then the S-parameters of the transition structures are de-embedded by the corresponding TRL calibration standards.

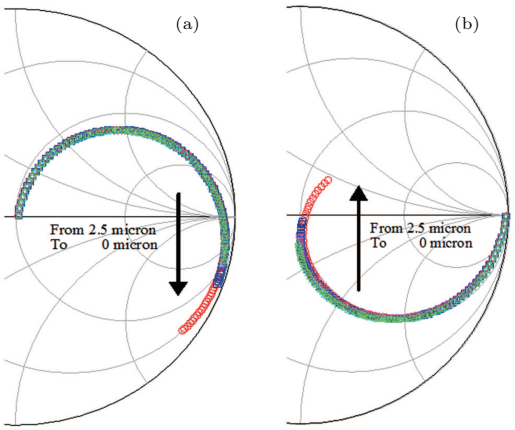


Fig. 2. (color online) The measured S-parameters for inductor 1 with the air-bridge heights of 0 μm, 0.1 μm, 0.5 μm, 1.0 μm, and 2.5 μm in the frequency range from 0.1 GHz to 60 GHz, (a) S_{11} and (b) S_{21}.

Figure 2 presents the measured S-parameters for inductor 1 with the line width of 4 μm and the gap width between lines of 4 μm. As it is indicated, with the air-bridge height decreasing, the measured S-parameters keep almost consistent in the lower frequency band, but vary significantly in the higher frequency band in the same direction.

Then the measured two-port parameters are transformed into one-port parameters by terminating one of the ports with a ground using the computer aided design software. The inductance is calculated by dividing the imaginary part of the input impedance (inductive stored energy) by the angular frequency assuming that the effect of the parasitic capacitance in the inductors at the frequencies much lower than the self-resonant frequency is negligible, as equation (1) shows. The unloaded Q-factor is determined by dividing the imaginary part (stored energy) of the input impedance by the real part (dissipated energy), as equation (2) shows.[13]

$$L = \frac{\mathrm{Im}(Z_{\mathrm{in}})}{\omega}, \tag{1}$$

$$Q = \frac{\mathrm{Im}(Z_{\mathrm{in}})}{\mathrm{Re}(Z_{\mathrm{in}})}. \tag{2}$$

Figure 3 shows the calculated L and Q-factor for the inductors with different air-bridge heights, and the details are shown in Table 1. As figure 3(a) shows, the inductor with the air-bridge height of 2.5 μm demonstrates a self-resonant frequency high up to 51.6 GHz. With the air-bridge height decreasing, the

strong coupling effect of the air-bridge can significantly deteriorate the self-resonant frequency which is moved from 51.6 GHz to 42.1 GHz. So with a lower height, the operating frequency band of the spiral inductor is narrowed down which is undesired in high frequency and wideband applications.

The deterioration of the self-resonant frequency can also be seen from the Q-factor curves as shown in Fig. 3(b). When the Q-factor curve crosses the zero line, the self-resonant frequency is reached, which is consistent with Fig. 3(a). When the air-bridge height is decreased, the peak Q-factor decreases from 12.14 to 11.13 and the corresponding frequency moves from 22.1 GHz to 17.6 GHz. So with the coupling effect of the air-bridge weakened, the Q-factor can be improved further.

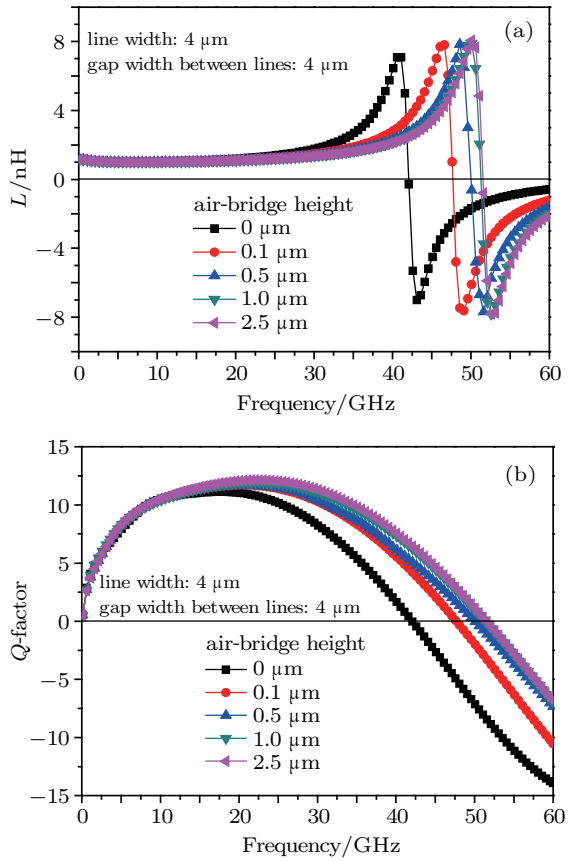


Fig. 3. (color online) The calculated (a) inductance, and (b) Q-factor of Inductor 1 with different air-bridge heights.

Table 1 shows the calculated results for the inductors with different dimensions. With the air-bridge height decreasing from 2.5 μm to 0 μm, the inductance values increase. The larger inductance value for lower air-bridge height indicates the strong coupling effect between the air-bridge and the underpass line which can result in the increase of the mutual inductance. Compared to inductor 1, inductor 3 with larger dimension exhibits a more significant variation in the amplitude because the overlapped area between the top spiral metal and the underpass line is larger. Moreover, when the air-bridge is higher than 0.5 μm, the inductance is almost constant which indicates that the coupling effect of the air-bridge is negligible. When the air-bridge height is decreased, the Q-factor and SRF of inductors 2 and 3 present the same variation tendency as inductor 1, which demonstrates the existence and the functions of the coupling effect.

Table 1. The characteristics of the on-chip spiral inductors with different air-bridge heights.

Microstrip and gap width/μm	Air-bridge height/μm	L/nH @5 GHz	SRF /GHz	Q peak /(@f GHz)
Inductor 1 4×4	0	1.02	42.1	11.13 (17.6)
	0.1	1.01	47.6	11.71 (20.6)
	0.5	1.00	50.1	11.89 (20.6)
	1	1.00	51.2	11.92 (22.1)
	2.5	1.00	51.6	12.14 (22.1)
Inductor 2 8×8	0	1.51	22.3	12.84 (12.4)
	0.1	1.49	28	13.87 (12.6)
	0.5	1.48	30	14.23 (13.1)
	1	1.47	30.3	14.36 (13.1)
	2.5	1.47	30.7	14.46 (13.1)
Inductor 3 12×12	0	2.49	12.8	12.69 (5.1)
	0.1	2.36	15.8	13.83 (7.1)
	0.5	2.29	17.7	14.33 (7.6)
	1	2.27	17.8	14.40 (7.6)
	2.5	2.27	18.3	14.42 (8.1)

Figure 4 shows the L dependence of the air-bridge for different inductors, which is in accordance with Table 1. To explain the variation quantitatively, equation (3) is applied to fit the original curves, which can effectively describe the exponential decay variation.

$$y = A_0 \cdot \exp\left(\frac{-x}{k_0}\right) + y_0. \tag{3}$$

In Eq. (3), y_0 is the displacement value in the y direction from the X axis, which stands for the inductance value. A_0 is a correction factor for the variation of the inductance amplitude. k_0 is a scalability factor in the X-axis direction which can characterizes the climb rate of L when the air-bridge height varies.

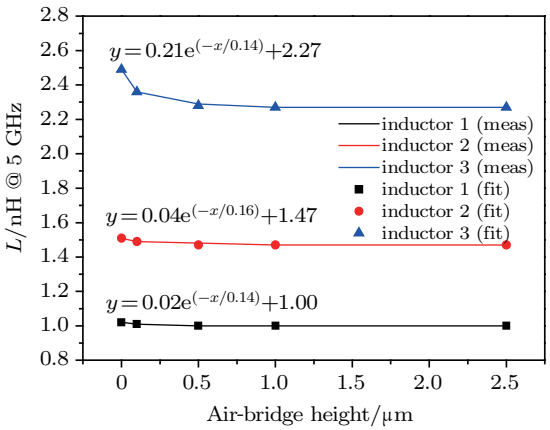


Fig. 4. (color online) The L dependence of the air-bridge height for different inductors.

As figure 4 indicates, when the inductance dimension is increased, y_0 will increases which equals to the inductance

in the lower frequency. A_0 becomes larger because the air-bridges cover more area, resulting in a stronger coupling effect, and the amplitude of the inductance varies more severe. Additionally, when the overlapped area between the air-bridge and the underpass line is enlarged, k_0 is almost the same. This is because there exists interaction between A_0 and k_0, and the variation of k_0 is not significant enough. To observe the meaning of k_0, more inductor samples with different dimensions should be fabricated and measured carefully.

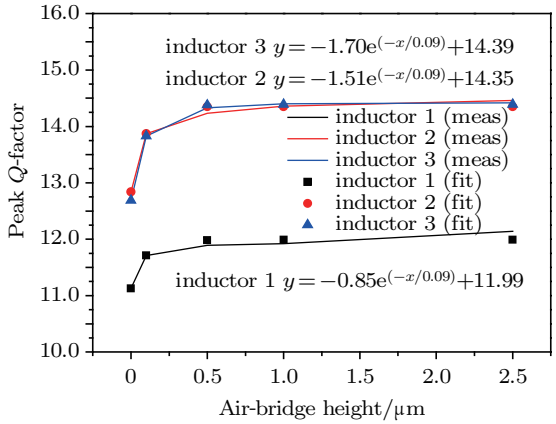


Fig. 5. (color online) The Q-factor dependence of the air-bridge height for different inductors.

Figure 5 presents the Q-factor dependence of the air-bridge height for different inductors. The original data can also be exactly fitted by Eq. (3), and the coefficients have the same meaning for Q-factor. As it is indicated in Fig. 5, the peak Q-factor which is represented by y_0 has an optimum value when the dimensions increase to a certain degree like inductors 2 and 3. The variation of A_0 also demonstrates the fact that the coupling effect will become stronger with the dimensions increasing and the amplitude of Q-factor will decrease more rapidly.

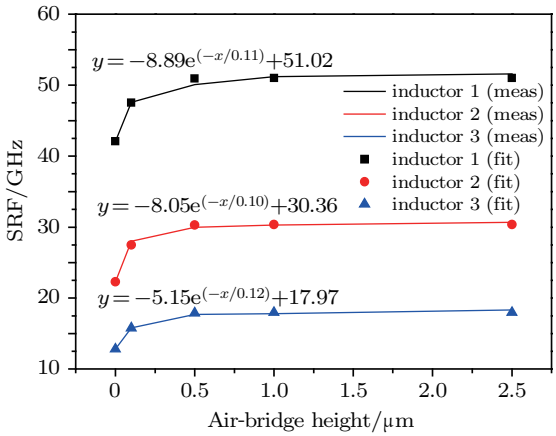


Fig. 6. (color online) The SRF dependence of the air-bridge height for different inductors.

In Fig. 6, the SRF dependence of the air-bridge height for different inductors is plotted, and equation (3) can also explain the relation between SRF and the air-bridge height exactly. In this relationship, y_0 stands for the SRF when the air-bridge is high enough and its coupling effect can be neglected. A_0 and k_0 account for the amplitude correction and the climb rate of SRF respectively when the air-bridge height is varied. When the dimensions of the inductor are decreased, the level of the SRF is raised significantly, and the variation of the SRF is steeper which can be reflected by A_0.

3. The parasitic capacitor in the lumped model for coupling effect

To investigate the coupling effect more deeply, a lumped element equivalent model has been established and the parameters have been extracted to study the parasitic effect separately.[1] Compared to Ref. [1], two lumped inductors L_{s1}/L_{s2} are added to characterize the input and output terminal connection microstrip, and the calculation for the coupling capacitor C_p is modified due to the multi-component dielectric between the air-bridge and the underpass line. Figure 7(a) shows a comprehensive lumped elements equivalent circuit for the on-chip spiral inductor. The main inductor is represented by L_m. The conductor loss is simulated by R_s. C_{g1}/C_{g2} can fit the capacitor between the spiral inductor and the back ground, and R_{g1}/R_{g2} can fit the substrate loss.

The lumped L_{s1} and L_{s2} can be deduced by fitting the S-parameters between the lumped inductors and the interconnection microstrip at the input and output terminals in CAD tools. After L_{s1} and L_{s2} is de-embedded, the data are converted to Y-parameter and the equivalent circuit is shown in Fig. 7(b), in which the circuit can be divided into three main parts, and expressed by Eqs. (4), (5), and (6)

$$Y_a = Y_{11} + Y_{21}, \tag{4}$$

$$Y_b = Y_{22} + Y_{21}, \tag{5}$$

$$Y_c = -Y_{21} = -Y_{12}. \tag{6}$$

With the specific value of Y_a and Y_b, the components in them could be determined by Eqs. (7)–(10).

$$R_{g1} = \frac{1}{\mathrm{Re}(Y_a)}, \tag{7}$$

$$C_{g1} = \frac{\mathrm{Im}(Y_a)}{2\pi f}, \tag{8}$$

$$R_{g2} = \frac{1}{\mathrm{Re}(Y_b)}, \tag{9}$$

$$C_{g2} = \frac{\mathrm{Im}(Y_b)}{2\pi f}, \tag{10}$$

where, Re and Im mean taking the real part and the imaginary part, respectively. In the Y_c part, there are two reactive elements which cannot be calculated directly, so one of them should be determined first. Assuming that C_p is only formed by the capacitor between the air-bridge and the underpass line,

and the formed capacitor is an ideal parallel-plate capacitor which can be obtained by Eq. (11).

$$C_{\rm p} = \frac{\varepsilon_{\rm eff} \cdot S}{d}, \tag{11}$$

where S is the cross-over area between the air-bridge and underpass line, d is the height of the total thickness of the air layer and the SiN layer under the air-bridge, and $\varepsilon_{\rm eff}$ is the effective dielectric constant which can be obtained by Lichtenecker formulation,[14] as equation (12) shows.

$$\varepsilon_{\rm eff}^{k} = v\varepsilon_{1}^{k} + (1-v)\varepsilon_{2}^{k}, \tag{12}$$

where $\varepsilon_{\rm eff}$ is the effective dielectric constant of the composite, ε_1 and ε_2 are the dielectric constants of the individual elements in the composite, v is the volume fraction of the first element, and when the elements are connected in series, k equals 1.

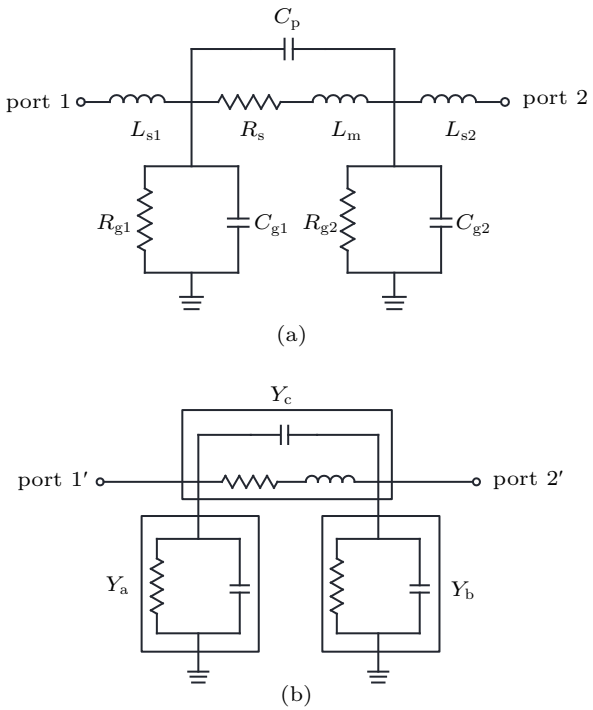


Fig. 7. (a) The lumped element model for the on-chip spiral inductors, and (b) the equivalent circuit after $L_{\rm s1}$ and $L_{\rm s2}$ are de-embedded.

With $C_{\rm p}$ determined, $L_{\rm m}$ and $R_{\rm s}$ can be calculated by Eqs. (13) and (14).

$$L_{\rm m} = {\rm Im}\left(\frac{-1}{Y_{21} + {\rm j}\cdot\omega C_{\rm p}}\right)/\omega, \tag{13}$$

$$R_{\rm s} = {\rm Re}\left(\frac{-1}{Y_{21} + j\cdot\omega C_{\rm p}}\right). \tag{14}$$

With the calculated initial value, the model is then optimized by gradient algorithm until the local minimum error is reached.

Figure 8 shows the extracted parameters for the 4-turns spiral inductors with different air-bridge heights. The parameters that do not appear in Fig. 8 are almost independent of the air-bridge height.

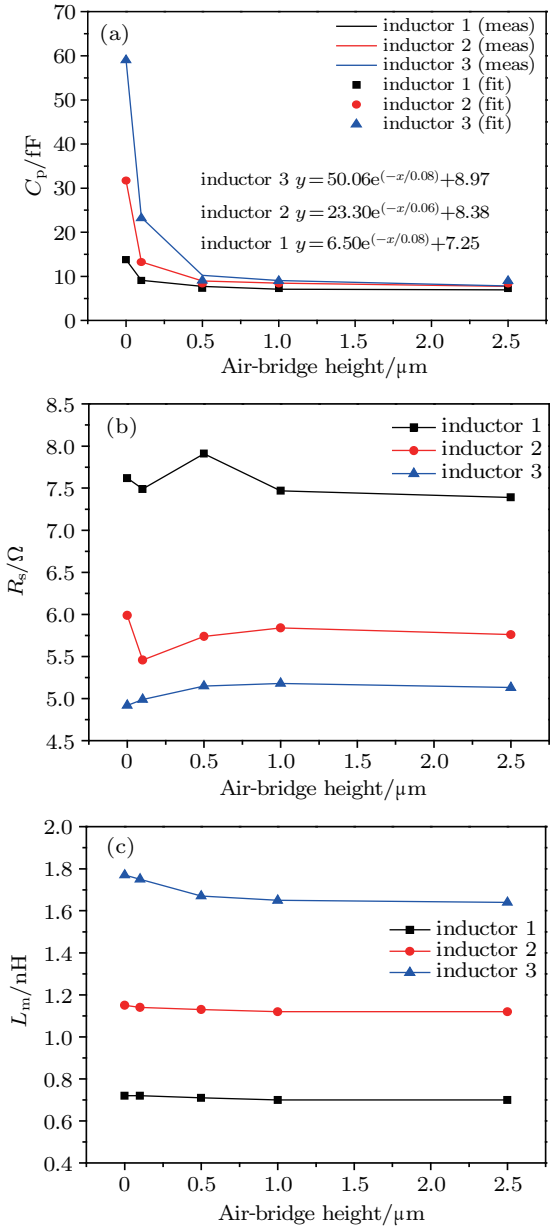


Fig. 8. (color online) The extracted parameters of the lumped model for different spiral inductors, (a) $C_{\rm p}$, (b) $R_{\rm s}$, and (c) $L_{\rm m}$.

Figure 8(a) shows the extracted $C_{\rm p}$ of different inductor with different air-bridge heights. The value of $C_{\rm p}$ which represents the coupling effect consists of two parts. One part is resulted from the coupling effect between the microstrip lines which can be determined when the air-bridge height is high enough and its coupling effect can be neglected. This part will remain constant for the same inductor dimension, and independent of the air-bridge height. The other part is contributed from the coupling effect of the air-bridge. Take inductor 1 as an example. When the air-bridge height is decreased, $C_{\rm p}$ increases significantly from 6.93 fF to 13.75 fF. Compared with inductor 1, inductors 2 and 3 with larger dimensions present the same regularity. And with the dimensions of the spiral inductors increasing, the area under the air-bridge becomes larger, resulting in a larger coupling capacitor,

which can be deduced from the capacitance expression of the parallel-plate capacitors. Moreover, the variation of C_p with the air-bridge height also presents the principle of exponential decay. The curves can be well fitted by Eq. (3), and the fitted results is shown in Fig. 8(a). With the dimensions of the inductor increasing, A_0 increases rapidly, and the amplitude of C_p varies more significantly because of the larger parasitic capacitor area. y_0 stands for the C_p when the air-bridge is high enough and its coupling effect can be neglected.

The variation of R_s is almost independent of the air-bridge height, but the value is not constant as figure 8(b) shows. Concerning a single inductor, R_s is randomly distributed in a small range when the air-bridge height varies. This is resulted from the gradient optimizing algorithm for the parameter optimizing and R_s is a fitting value which is distributed in a reasonable range. But compared with inductor 1, inductor 3 with a larger dimension has smaller R_s because the wider microstrip possesses lower resistivity.

Compared with L in Table 1, the extracted L_m in Fig. 8(c) is smaller. This is because in the lumped model in Fig. 7(a), the inductive components consist of L_{s1}, L_{s2}, and L_m. And when compared to $(L_{s1}+L_{s2}+L_m)$, the calculated L in Table 1 has a comparable value. Additionally, when the air-bridge height decreases, the it gets closer to the underpass line, and the coupling effect become stronger. Then L_m increases with the mutual inductance gaining, which is in accordance with the result in Table 1.

4. The field distribution results by electromagnetic simulations for the air-bridge

To further investigate the coupling effect of the air-bridge, the electromagnetic simulation based on the finite element method (FEM)[15] is performed and the field distribution results are discussed. Figure 9 shows the electric field distribution results for inductor 1 with different air-bridge heights. The flat top metal accounts for the major area of the air-bridge and the maximum electric field intensity (E_m) of the air-bridge is focused here, which makes the main contributions to the coupling effect. So the electric field intensity under the flat top metal for different air-bridges is discussed detailedly.

Figure 9(a) shows the electric field distribution for inductor 1 with a 0-μm-high air-bridge. Because the air-bridge, the SiN and the underpass line metal have formed an MIM capacitor, the electric field is strong in the dielectric layer, and the maximum electric field intensity is almost 7.31×10^7 V/m, which indicates the existence of strong coupling effect and deteriorates the frequency performance and the Q-factor significantly. Figure 9(b) shows the electric field distribution results for inductor 1 with a 0.5-μm-high air-bridge. With the existence of a 0.5-μm-thick air layer, the maximum electric field intensity is 6.46×10^6 V/m in SiN and as high as 2.42×10^7 V/m in the air layer. The coupling capacitor is reduced to 7.75-fF compared with 13.75 fF when the height is zero. With the height lifted to 2.5 μm as figure 9(c) shows, the air layer is thicker, the maximum electric field intensity is weakened to 1.77×10^6 V/m in the SiN dielectric, and the coupling capacitor is reduced to 6.93 fF, which is mainly resulted from the coupling effect between the lines. In this condition, the coupling effect of the air-bridge can be neglected.

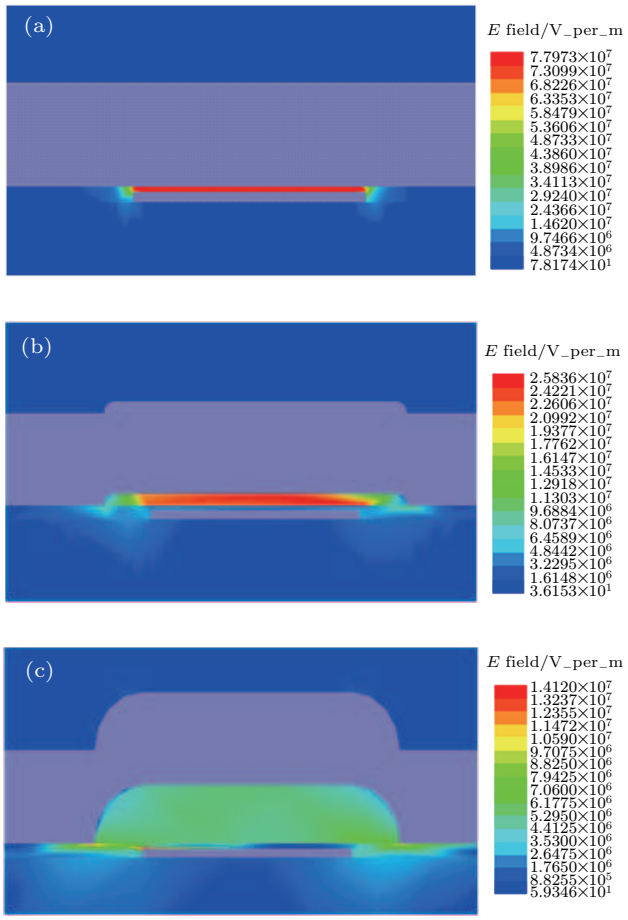


Fig. 9. (color online) The electric field distribution results for inductor 1 with the air-bridge heights of (a) 0 μm, (b) 0.5 μm, and (c) 2.5 μm.

In Fig. 10, the maximum electric field intensity of spiral inductors with different dimensions are listed and compared according to the calculated results by the electromagnetic simulation software. When the air-bridge height is decreased, the maximum electric field intensity in SiN grows rapidly. The same phenomenon occurs in the air layer. When the air-bridge height is 0.1 μm, the E_m in the air is of the order of 10^8 V/m, much larger than the E_m in SiN when the height becomes zero. But the relative dielectric constant E_r of SiN is about 6.8, much larger than that of the air with the value of 1. So the coupling capacitor of the 0 μm-high air-bridge is still larger than that of the 0.1 μm-high air-bridge.

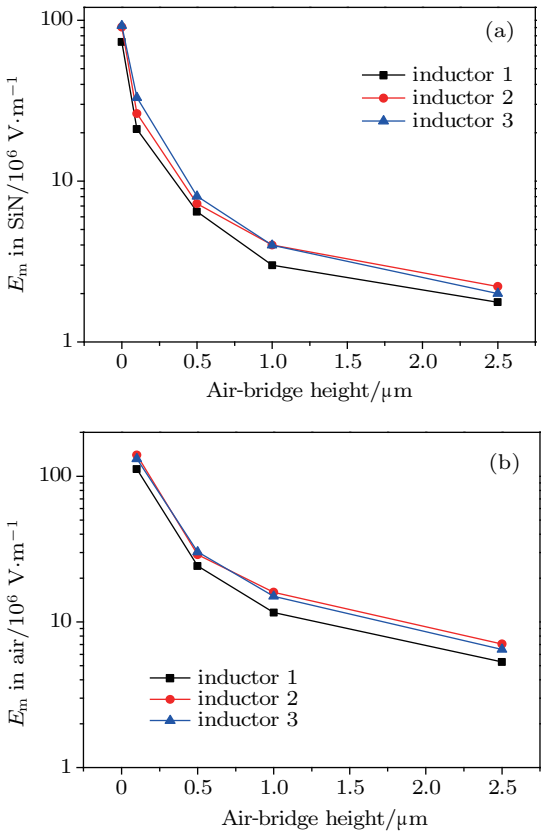


Fig. 10. (color online) The maximum electric field intensity (E_m) of the air-bridge with different heights, (a) E_m in SiN, and (b) E_m in air.

5. Conclusions

The planar broadband spiral inductors with air-bridges in SiC-based MMIC technology have been fabricated and studied. The 1-nH inductor shows a high self-resonant frequency of 51.6 GHz, with a peak Q-factor of 12.14 at 22.1 GHz. The coupling effect of the air-bridge in spiral inductors has been investigated deeply. The calculated results from the measured S-parameters show that the inductance, the self-resonant frequency and the Q-factor will deteriorate significantly with the air-bridge height decreasing. The exponential decay phenomenon is observed for L, Q, and SRF with the air-bridge height decreasing, and an analytic expression is concluded to fit the measured data exactly which can be used to predict the performance of the spiral inductor. All the coefficients in the formula have specific meaning. The relative lumped model and the electromagnetic field distribution is presented for the inductors with different air-bridge heights to explore its parasitic capacitor and the maximum electric field intensity variation, and the exponential decay phenomenon of the parasitic capacitor indicates that it is directly related to the coupling effect of the air-bridge.

References

[1] Fang M, Wang J Y, Lin S X, Meng D, Cai Y, Hao Y L and Wen C P 2011 *IEEE 4*th *International Symposium on Microwave, Antenna, Propagation, and EMC Technologies for Wireless Communications (MAPE)*, November 1–3, 2011, Beijing, China, p. 400
[2] Burghartz J N, Edelstein D C, Jenkins K A and Kwark Y H 1997 *IEEE Transactions on Microwave Theory and Techniques* **45** 1961
[3] Ribas R P, Lescot J, Leclercq J L, Bennouri N, Karam J M and Courtois B 1998 *IEEE Electron Dev. Lett.* **19** 285
[4] Shepherd P R 1986 *IEEE Transactions on Microwave Theory and Technique* **MTT-34** 467
[5] Tang Y, Liu B, Zhang L, Pan J, Yang L W and Wang Y 2008 *Solid-State Electron.* **52** 1058
[6] Teo T H, Choi Y B, Liao H L, Xiong Y Z and Fu J S 2004 *Solid-State Electron.* **48** 1643
[7] Hsu H M and Hsieh M M 2008 *Solid-State Electron.* **52** 998
[8] Cao M Y, Zhang K, Chen Y H, Zhang J C, Ma X H and Hao Y 2014 *Chin. Phys. B* **23** 037305
[9] Zheng J X, Ma X H, Lu Y, Zhao B C, Zhang H H, Zhang M, Cao M Y and Hao Y 2015 *Chin. Phys. B* **24** 107305
[10] Huo X, Chen K J and Chan P C H 2002 *IEEE Radio Frequency Integrated Circuits (RFIC) Symposium*, June, 2002, p. 403
[11] Zhang Z Q and Liao X P 2012 *IEEE Sensors Journal* **12** 1853
[12] Shih Y C, Pao C K and Itoh T 1992 *IEEE MTT-S International Microwave Symposium Digest*, June, 1–5, 1992, Albuquerque, NM, USA, **3** p. 1345
[13] Hettak K, Ross T, Elgaid K, Thayne I G and Wight J 2011 *Asia-Pacific Microwave Conference*, December 5–8, 2011, Melbourne, Australia, p. 1070
[14] Goncharenko A V, Lozovski V Z and Venger E F 2000 *Opt. Commun.* **174** 19
[15] Jin J M 2002 *The Finite Element Method in Electromagnetics* (New York: John Wiley & Sons. Inc.)